Supporting Information

Field-Induced Magnetic Relaxation in Heteropolynuclear Ln^{III}/Zn^{II} Metal Organic Frameworks: Cerium and Dysprosium Cases

Agustín López[a], Carlos Cruz[b,c], Verónica Paredes-García[b,c], Nicolás Veiga[a], Francesc Lloret[d], Julia Torres[a], Raúl Chiozzone[a,*]

a Universidad de la República, Facultad de Química, Área Química Inorgánica, Montevideo, Uruguay.
b Universidad Andrés Bello, Facultad de Ciencias Exactas, Departamento de Ciencias Químicas, Santiago, Chile.
c Center for the Development of Nanoscience and Nanotechnology, CEDENNA, Chile.
d Universitat de València, Instituto de Ciencia Molecular (ICMol), Valencia, Spain.

Keywords:
Cerium(III)-based single-molecule magnets
Ab initio computational calculations
Heteronuclear polycarboxylate-based metal-organic frameworks

Experimental

Synthesis of $[Ln_2Zn_3(oda)_6(H_2O)_6]\cdot 12H_2O$ (Ln = Ce (**1**), Gd (**3**))

$CeCl_3\cdot 7H_2O$ or $GdCl_3\cdot 6H_2O$ (0.125 mmol) and $ZnCl_2$ (0.188 mmol) dissolved in 1mL H_2O were mixed with 3 mL of an aqueous solution containing 0.375 mmol H_2oda at pH = 7.0-7.5. The resulting solution (pH = 6.1-6.5) was diffused with twice the volume of isopropanol. After some weeks, crystals of the desired complexes were obtained (Yield 20-30%). *Anal. Calc*. for $C_{24}H_{60}Ce_2O_{48}Zn_3$: C, 18.1; H, 3.8. Found: C, 18.3; H, 3.6. *Anal. Calc*. for $C_{24}H_{60}Gd_2O_{48}Zn_3$: C, 17.7; H, 3.7. Found: C, 17.8; H, 3.6. Vibration modes ν_{as}(COO), ν_s(COO) and ν(COC) of the free H_2oda at 1732, 1419 and 1149 cm^{-1} shifted to 1606, 1438 and 1126 cm^{-1} in both compounds.

Synthesis of $[Dy_2Zn_3(oda)_6(H_2O)_6]\cdot 16H_2O$ (**2a**)

$DyCl_3\cdot 6H_2O$ (0.125 mmol) and $ZnCl_2$ (0.188 mmol) dissolved in 1 mL H_2O were mixed with 3 mL of an aqueous solution containing 0.375 mmol H_2oda at pH = 7.0-7.5. The resulting solution (pH = 6.1-6.5) was diffused with an equal volume of isopropanol. Crystals of **2a** were obtained after some weeks (Yield 40-50%). *Anal. Calc*. for $C_{24}H_{68}Dy_2O_{52}Zn_3$: C, 16.9; H, 4.0. Found: C, 17.0; H, 3.9. Vibration modes ν_{as}(COO), ν_s(COO) and ν(COC) at 1606, 1438 and 1126 cm^{-1}.

Synthesis of $[Dy_2Zn_3(oda)_6(H_2O)_6]\cdot 3H_2O$ (**2b**)

$DyCl_3\cdot 6H_2O$ (0.125 mmol) and $ZnCl_2$ (0.188 mmol) dissolved in 1mL H_2O were mixed with 6 mL of an aqueous solution containing 0.375 mmol H_2oda at pH = 7.0-7.5. The resulting solution (pH = 6.1-6.5) was diffused with an equal volume of acetone. Crystals of **2b** were obtained after some weeks (Yield 40-50 %). *Anal. Calc*. for $C_{24}H_{42}Dy_2O_{39}Zn_3$: C, 19.5; H, 2.9. Found: C, 19.7; H, 3.1. Vibration modes ν_{as}(COO), ν_s(COO) and ν(COC) at 1606, 1438 and 1131 cm^{-1}.

Infrared spectra were recorded with a Shimadzu IR Prestige-21 FTIR spectrometer as KBr pellets in the 4000–400 cm^{-1} region. Elemental analyses for carbon, hydrogen and nitrogen were performed on a Thermo Flash 2000 analyzer.

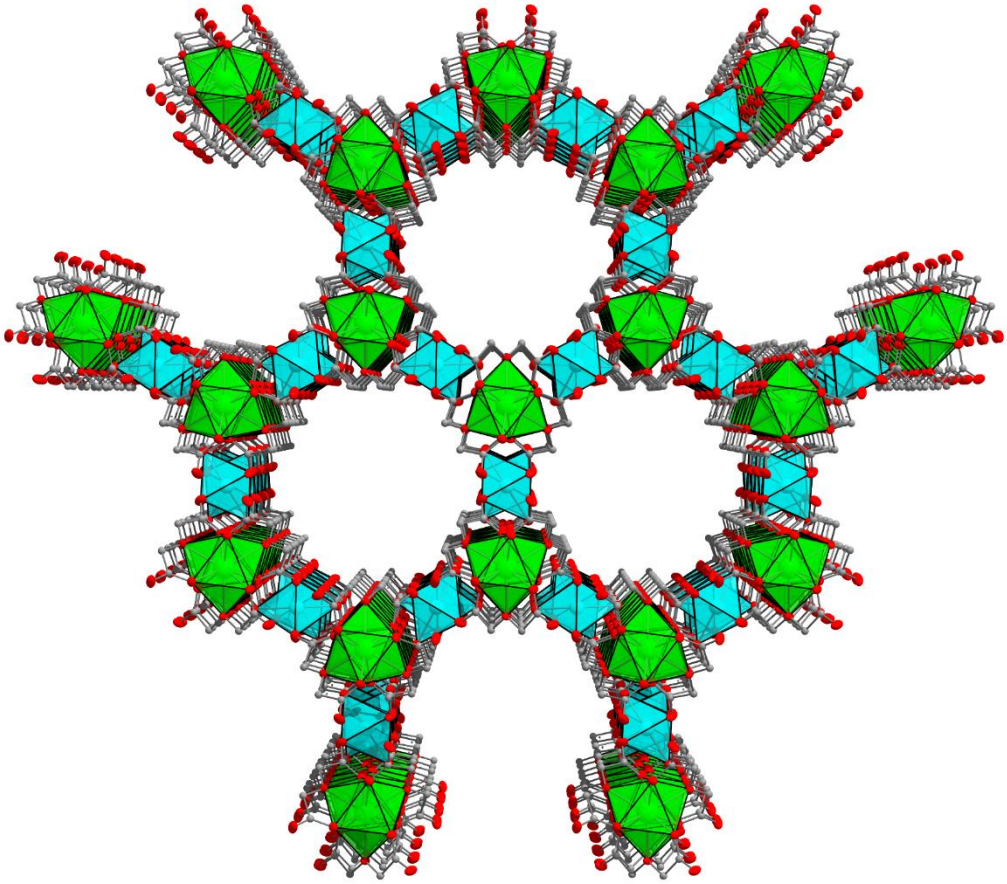

Figure S1. Perspective view along the *z*-axis showing the hexagonal network and nanochannels in **2a**. Color code: Dy green, Zn light blue, O red, C gray. Hydrogen atoms have been omitted for clarity.

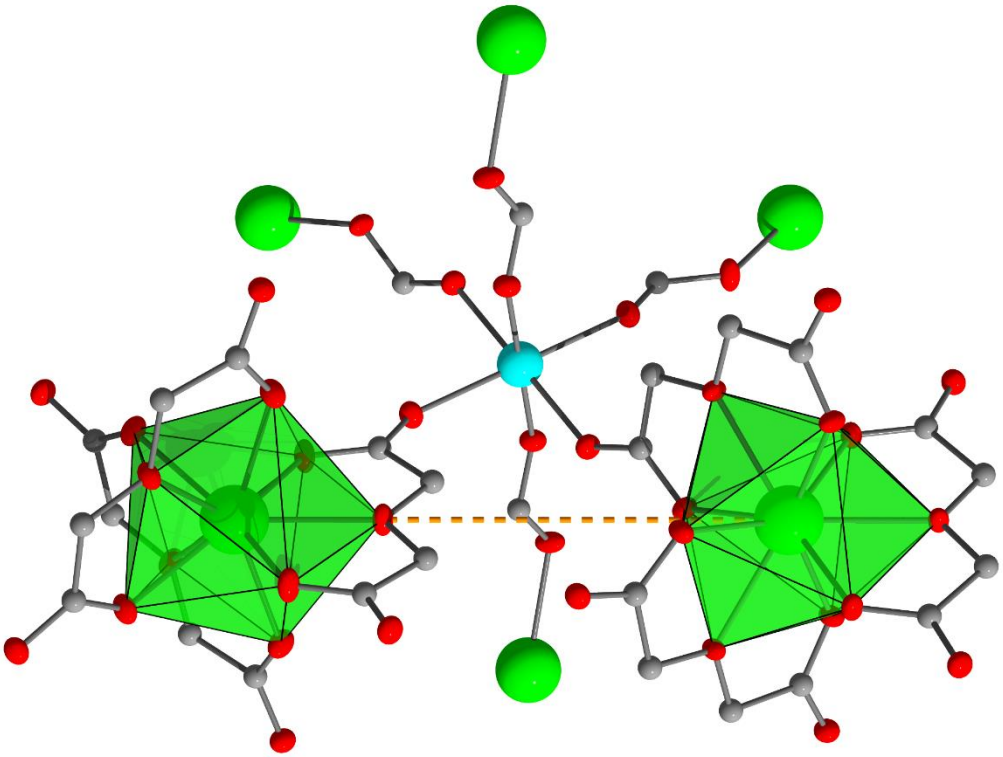

Figure S2. Tilted neighbouring $[Dy(oda)_3]^{3-}$units in **2b**. Color code: Dy green, Zn light blue, O red, C gray. Hydrogen atoms have been omitted for clarity. The slashed orange line indicates the shortest Dy···Dy distance.

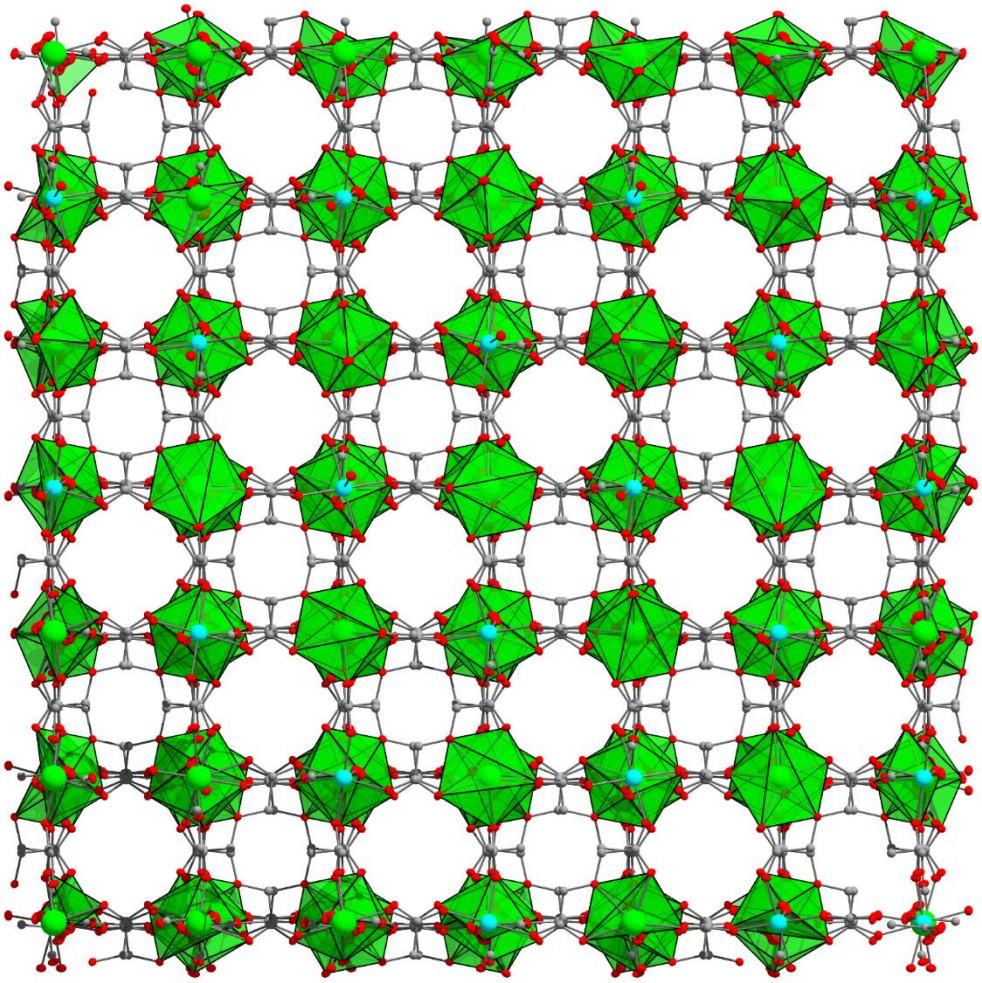

Figure S3. View along the *x*-axis of the anionic network $[\{ZnDy(oda)_3\}_2]^{2-}$ in **2b**. Color code: Dy green, Zn light blue, O red, C gray. Hydrogen atoms have been omitted for clarity.

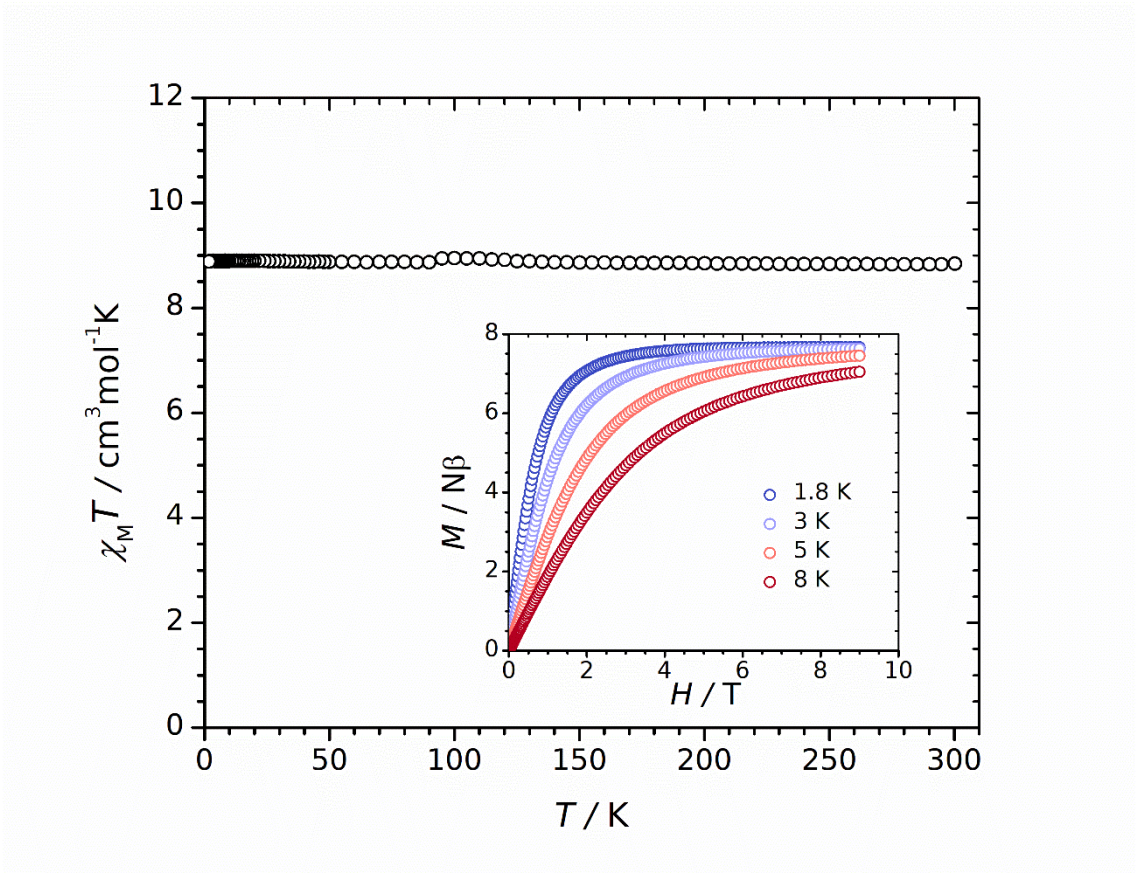

Figure S4. Temperature dependence of $\chi_M T$ measured at a 1 kOe dc field for **3**. Inset: Field dependence of magnetization at 1.8, 3.0, 5.0 and 8.0 K.

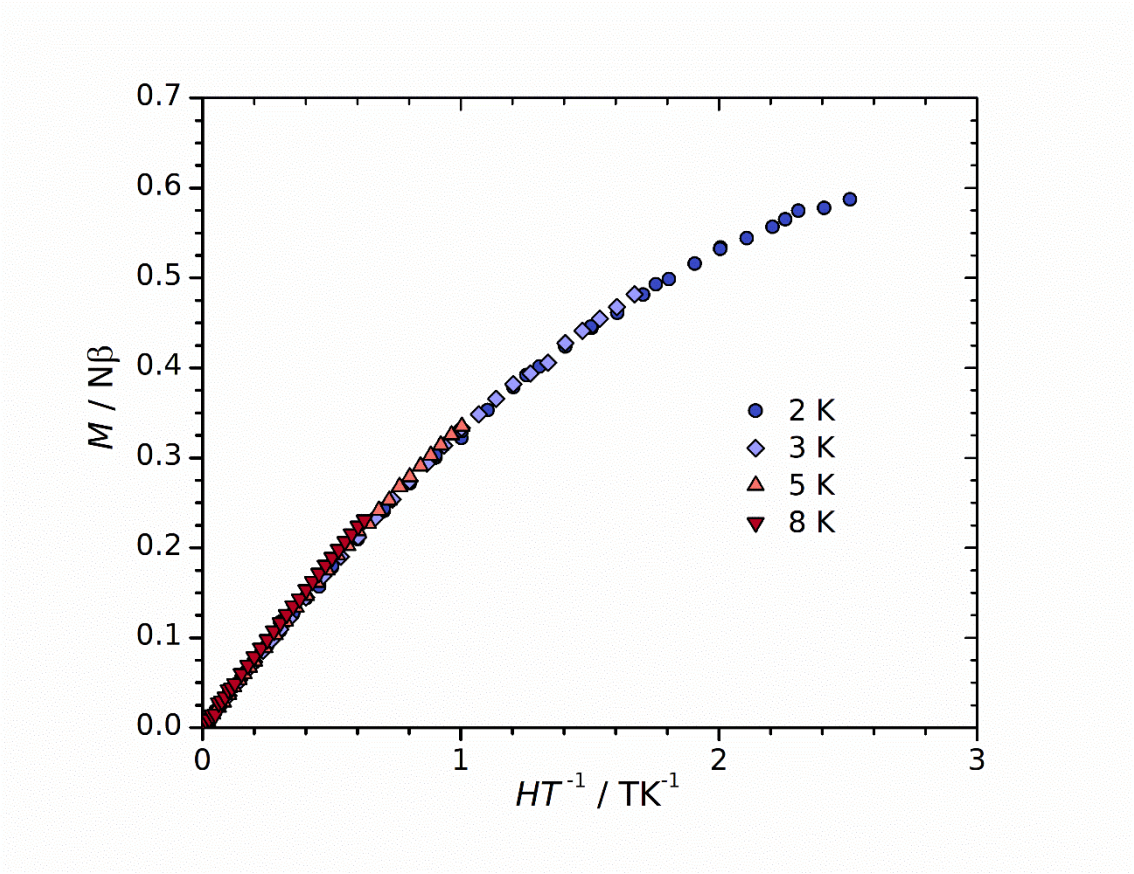

Figure S5. Reduced magnetization for compound **1** measured at 2.0, 3.0, 5.0 and 8.0 K.

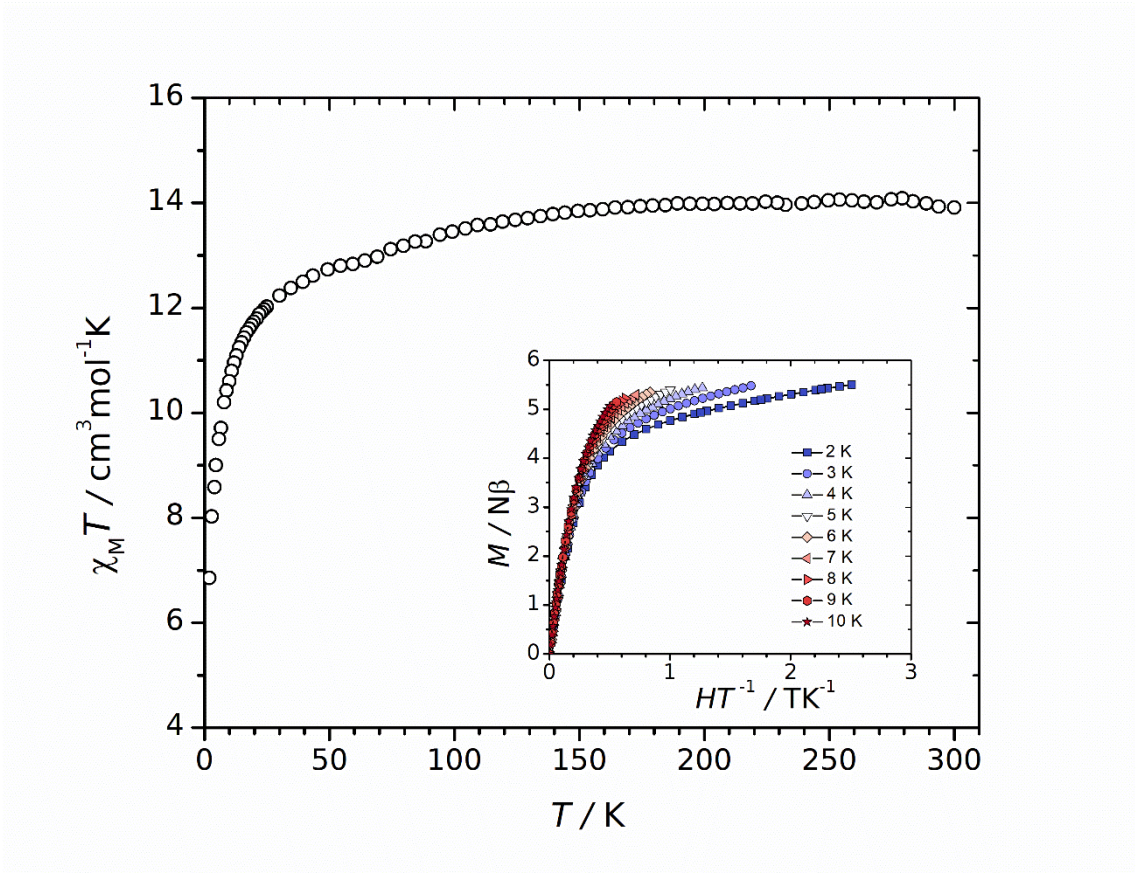

Figure S6. Temperature dependence of $\chi_M T$ measured at a 5 kOe dc field for **2b**. At 300 K, $\chi_M T$ is 13.9 cm^3 K mol^{-1}, very close to the expected 14.2 cm^3 K mol^{-1} value. Upon cooling, $\chi_M T$ decreases to 6.9 cm^3 K mol^{-1} at 2 K. Inset: Reduced magnetization measured between 2.0 and 10 K in steps of 1 K. The magnetization at 2 K reaches the value of 5.5 μ_B at 50 kOe.

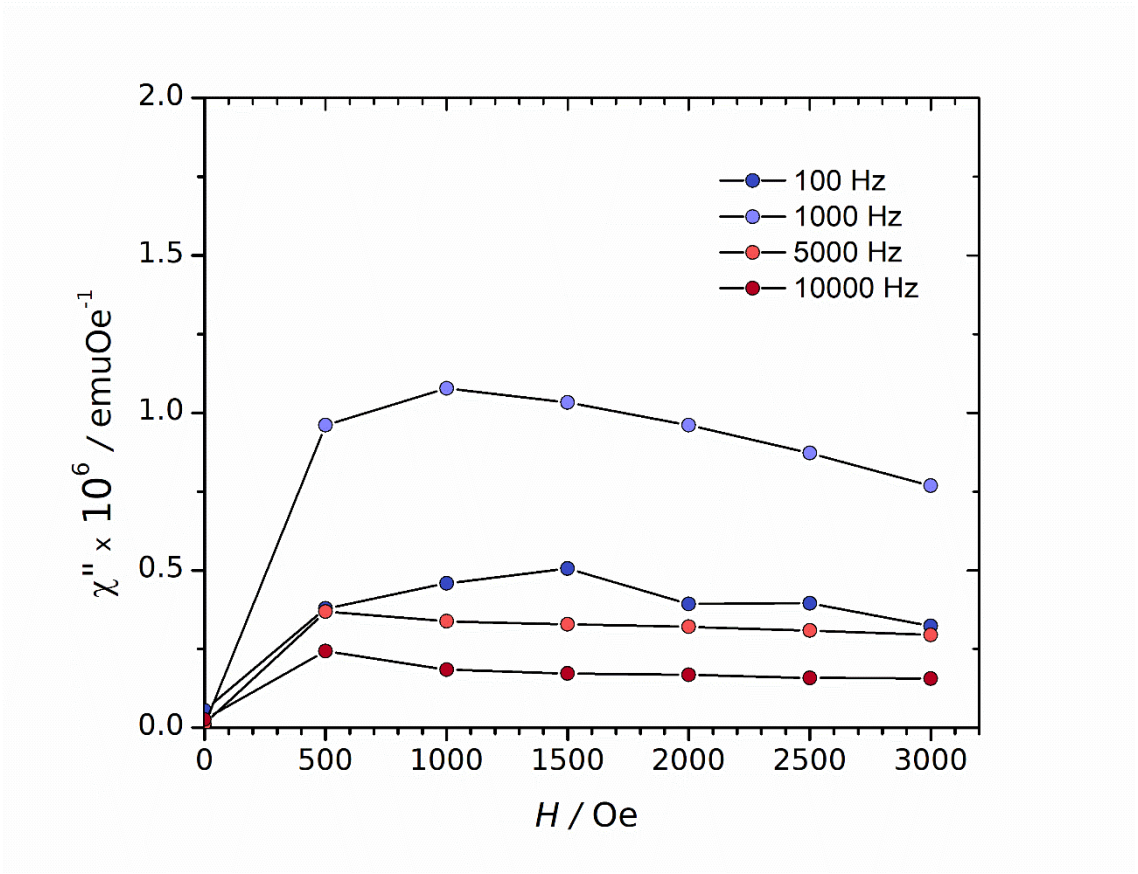

Figure S7. Static magnetic field dependence of the out-of-phase susceptibility of **1** at different frequencies of the oscillating *ac* field measured at 2.0 K. Lines serve only as a visual guide.

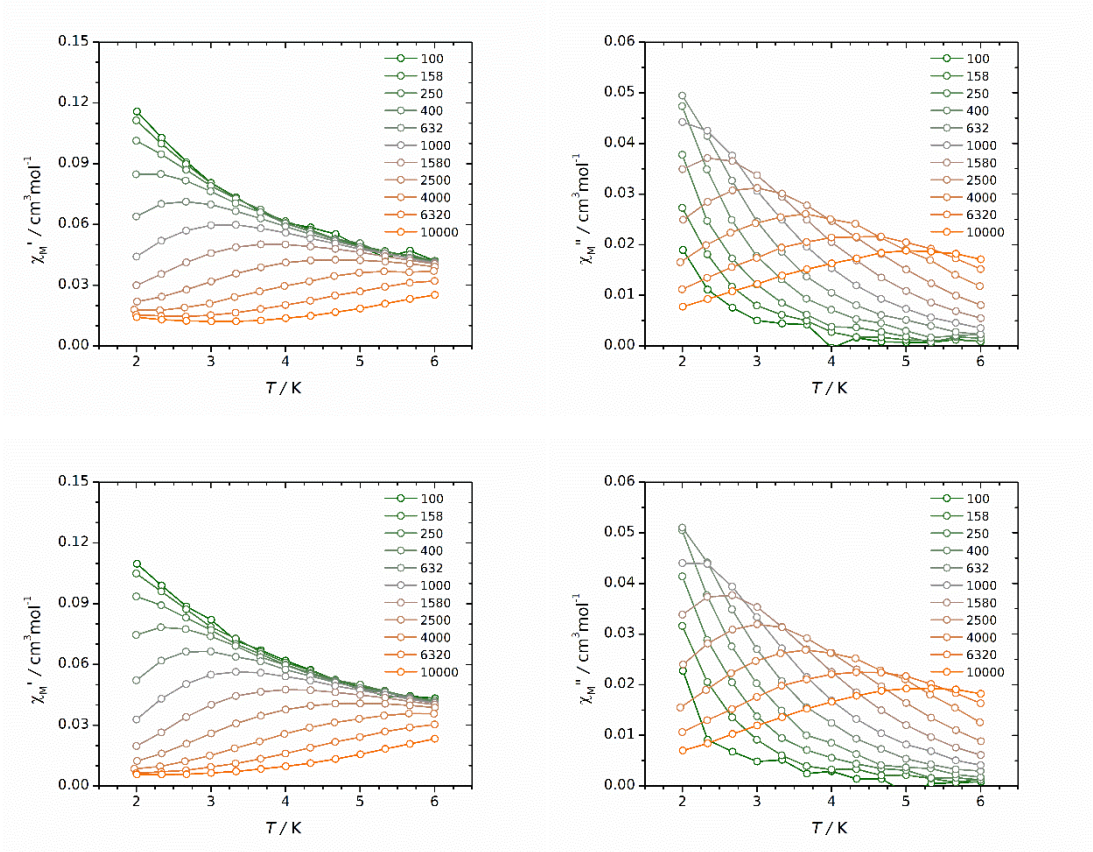

Figure S8. Temperature dependence of the *ac* susceptibility for **1** at static fields of 1 (top) and 2 kOe (bottom) at different frequencies between 100 and 10000 Hz. (left) in-phase components, (right) out-of phase components. Lines serve only as a visual guide.

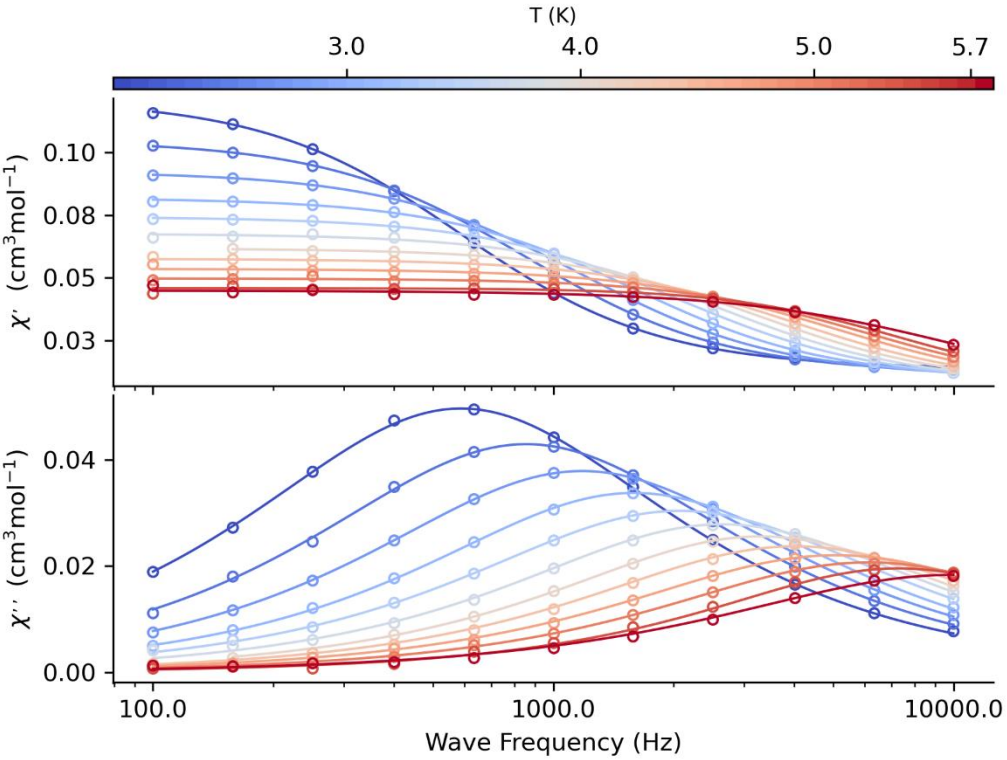

Figure S9. Frequency dependence of χ_M' and χ_M" at different temperatures for **1** under an external *dc* field of 1 kOe. The solid curves are theoretical calculations on the basis of the generalized Debye model. Temperature points for which a maximum is not observed were discarded.

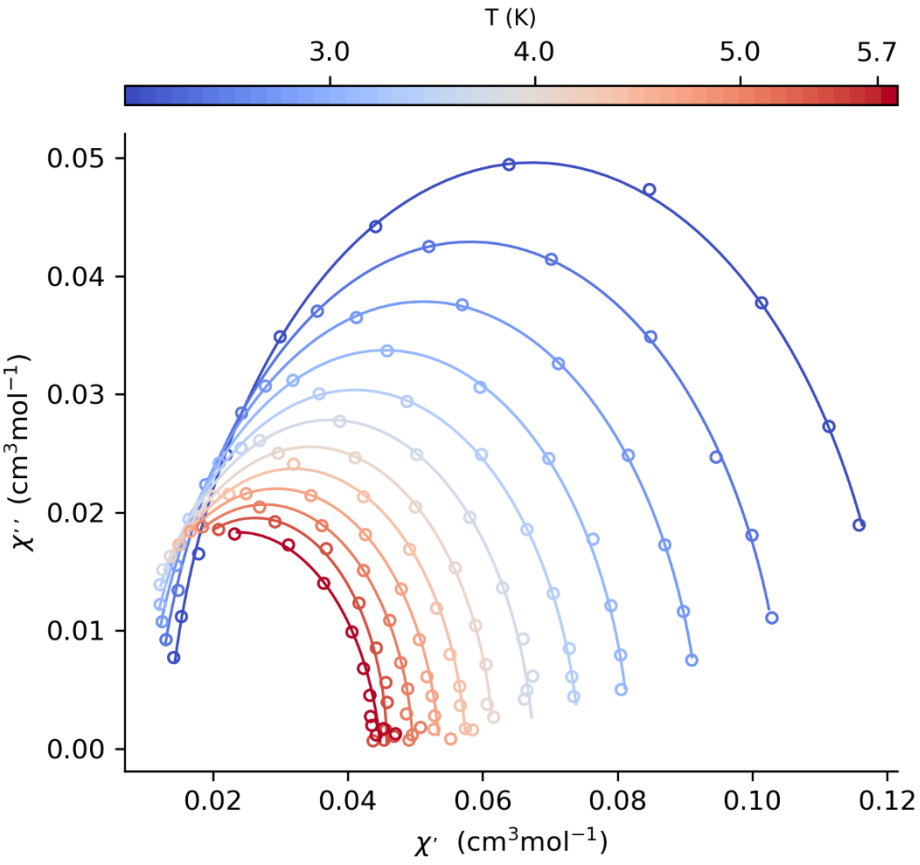

Figure S10. Argand diagram of **1** between 2.0 K (blue) and 5.7 K (red) under a *dc* field of 1 kOe. Lines represent the best fits as calculated with the generalized Debye model.

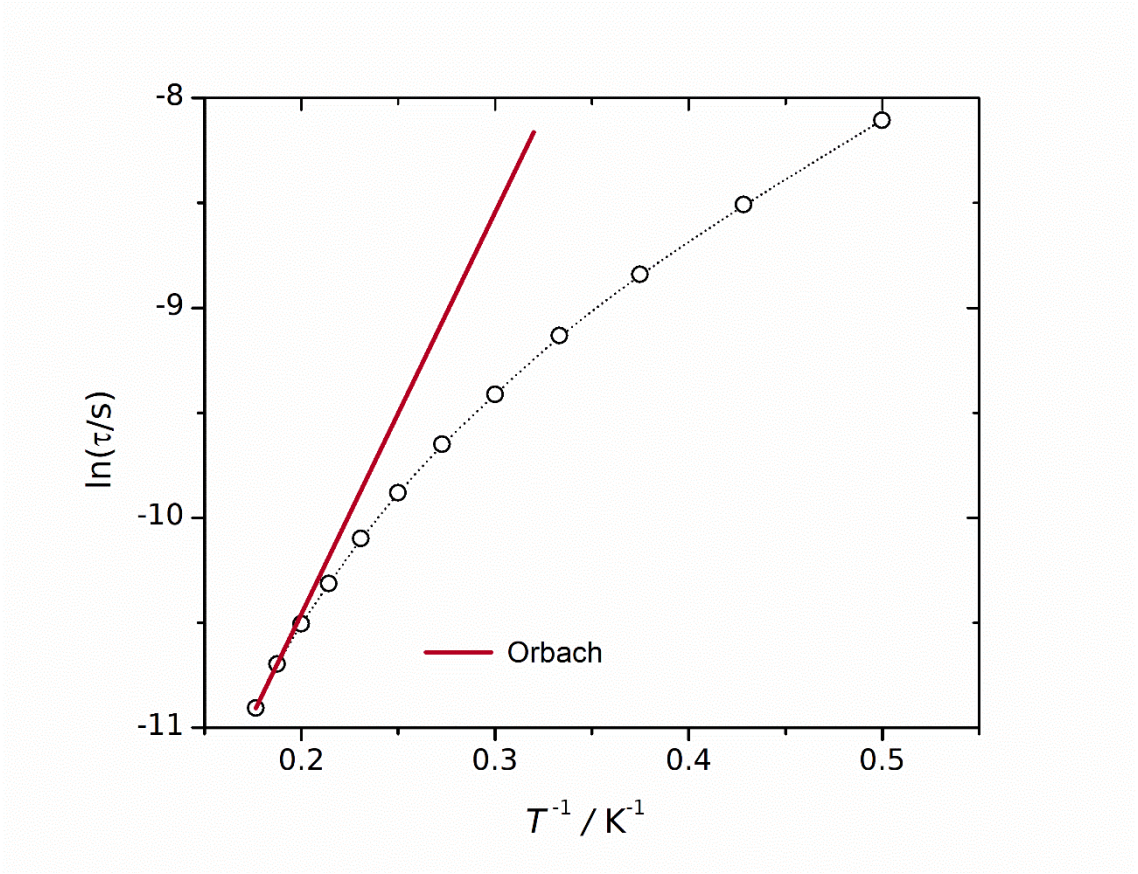

Figure S11. Arrhenius plot for **1** measured under a 2 kOe external field. An effective barrier of *ca*. 13 cm^{-1} (19 K) could be estimated from the slope of the red line as the Orbach contribution at the high temperature region.

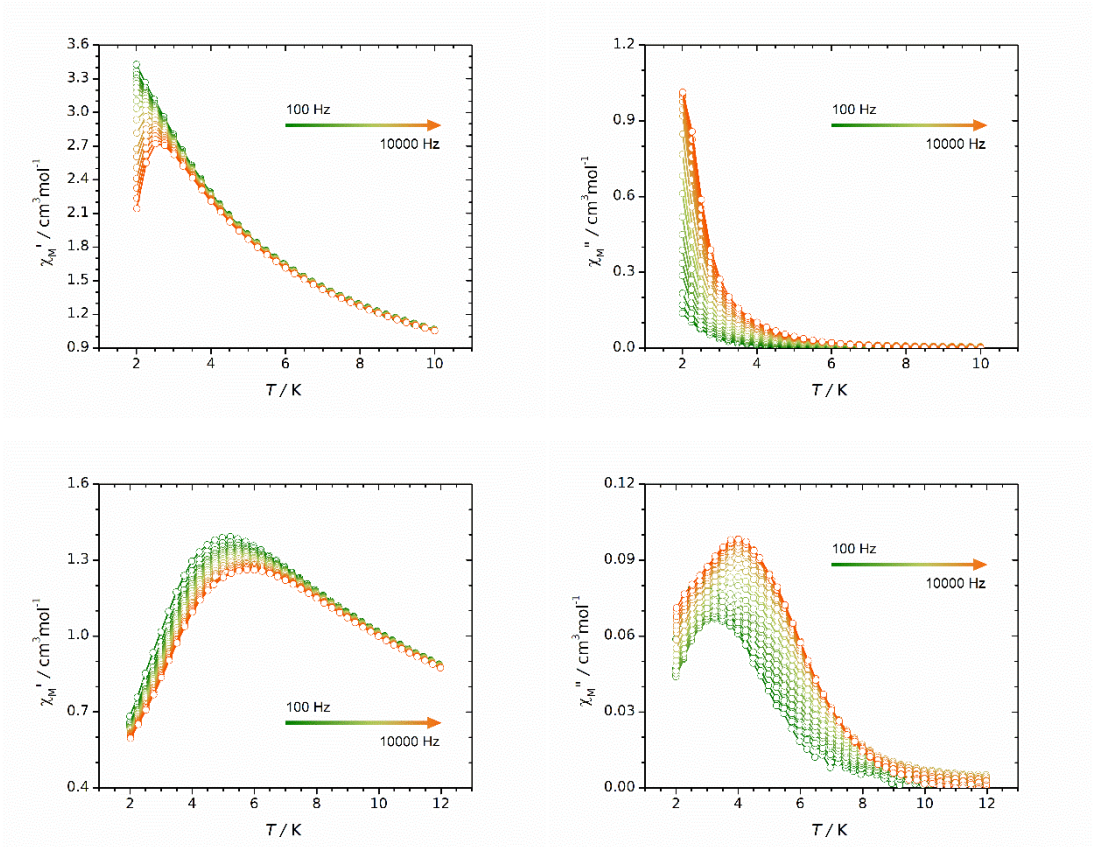

Figure S12. Temperature dependence of the *ac* susceptibility for **2a** at static fields of 1 (top) and 5 kOe (bottom) at different frequencies between 100 and 10000 Hz. (left) in-phase components, (right) out-of phase components. Lines serve only as a visual guide.

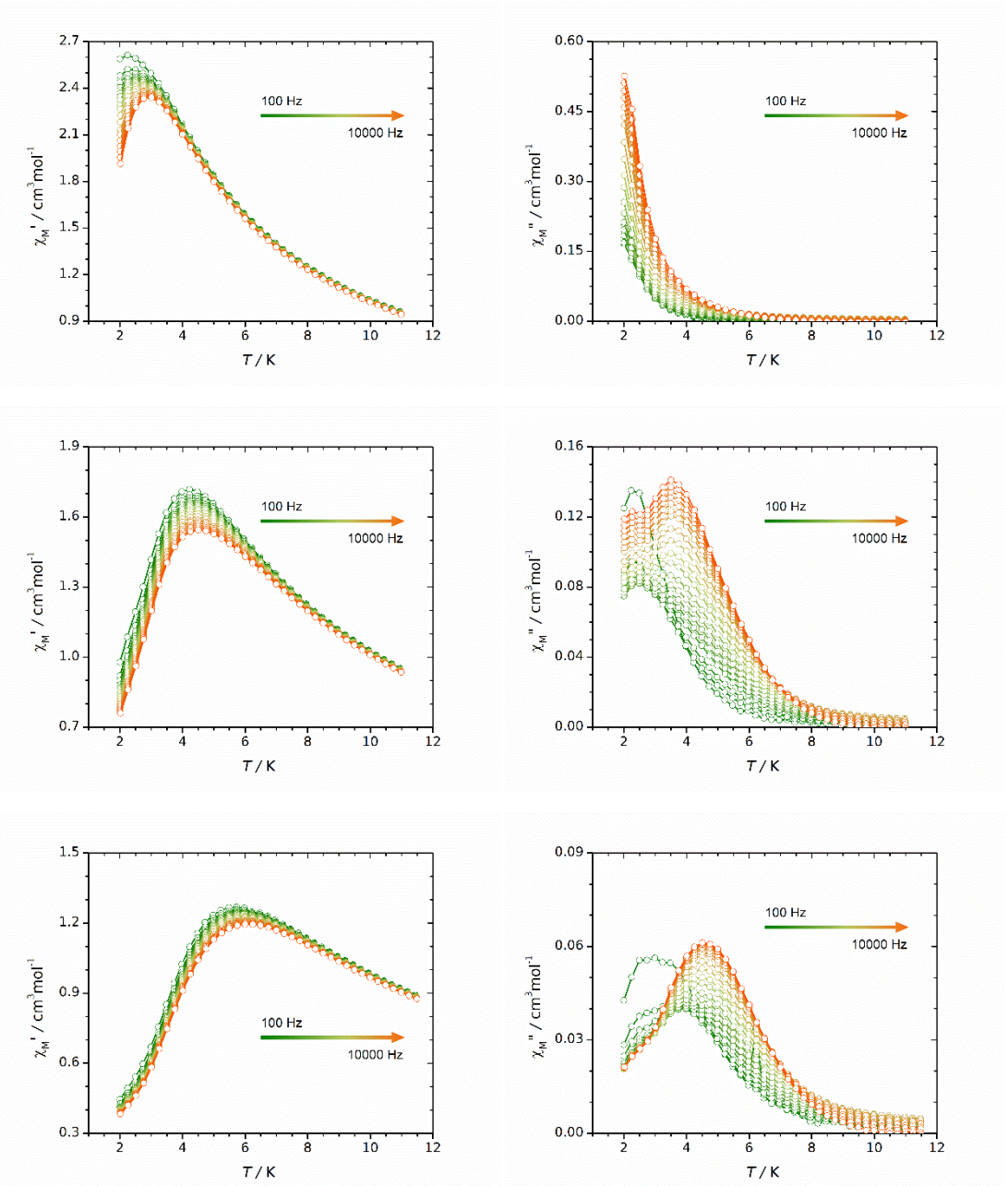

Figure S13. Temperature dependence of the *ac* susceptibility for **2b** at static fields of 1 (top), 2.5 (middle) and 5 kOe (bottom) at different frequencies between 100 and 10000 Hz. (left) in-phase components, (right) out-of phase components. Lines serve only as a visual guide.

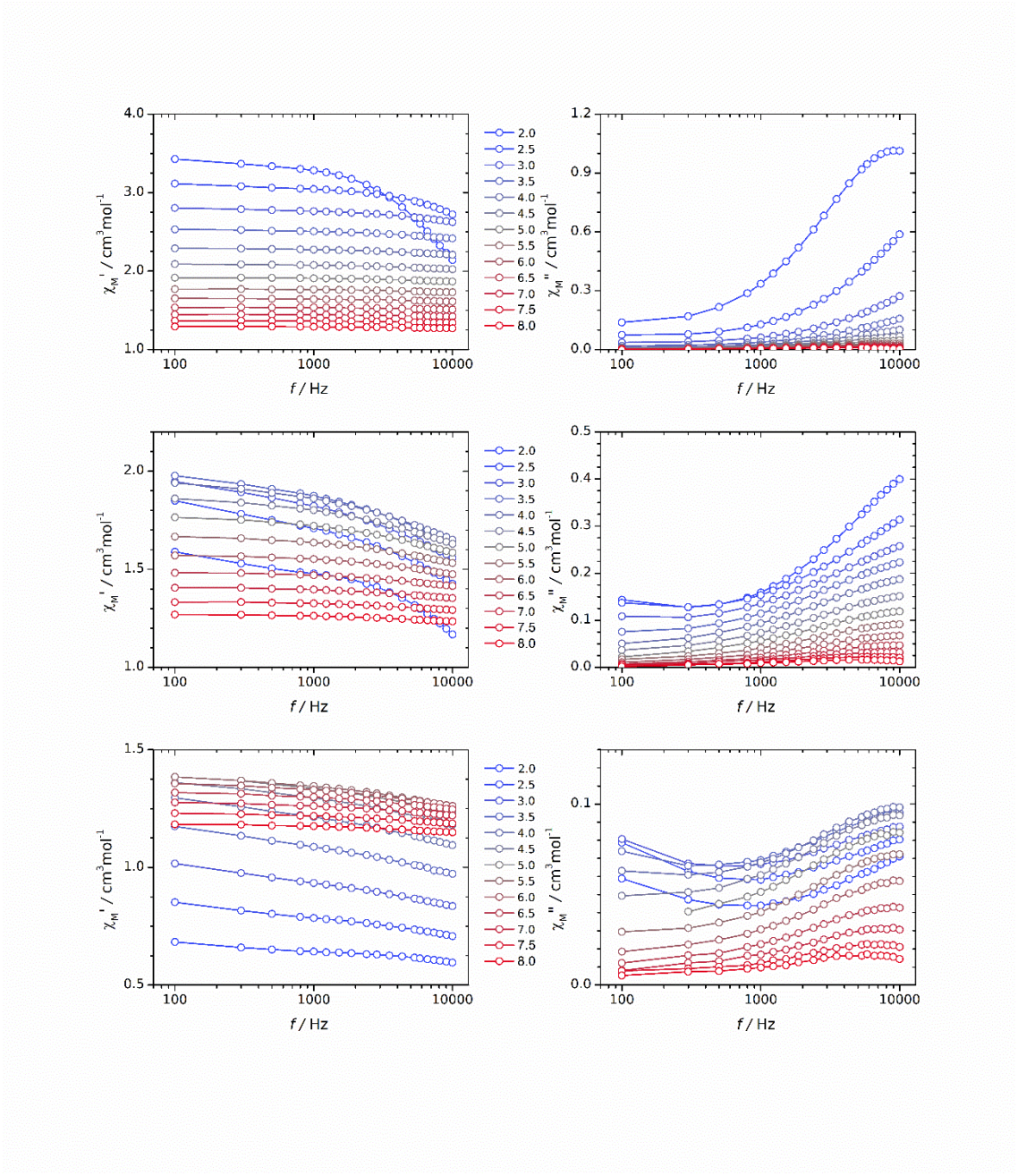

Figure S14. Frequency dependence of χ_M' (left) and χ_M'' (right) at different temperatures for **2a** under an external *dc* field of 1 (top), 2.5 (middle) and 5 kOe (bottom). Lines serve only as a visual guide.

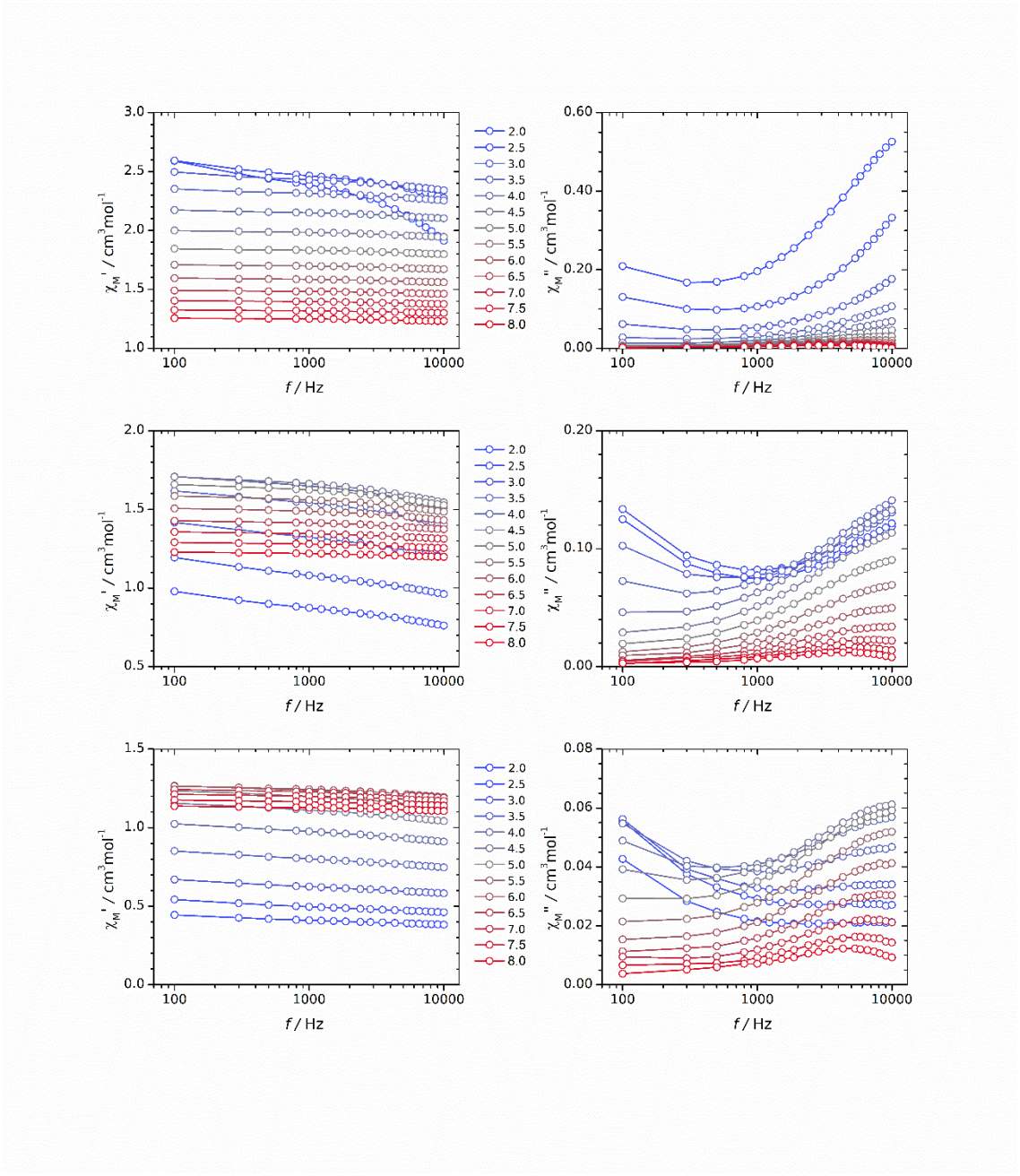

Figure S15. Frequency dependence of χ_M' (left) and χ_M" (right) at different temperatures for **2b** under an external *dc* field of 1 (top), 2.5 (middle) and 5 kOe (bottom). Lines serve only as a visual guide.

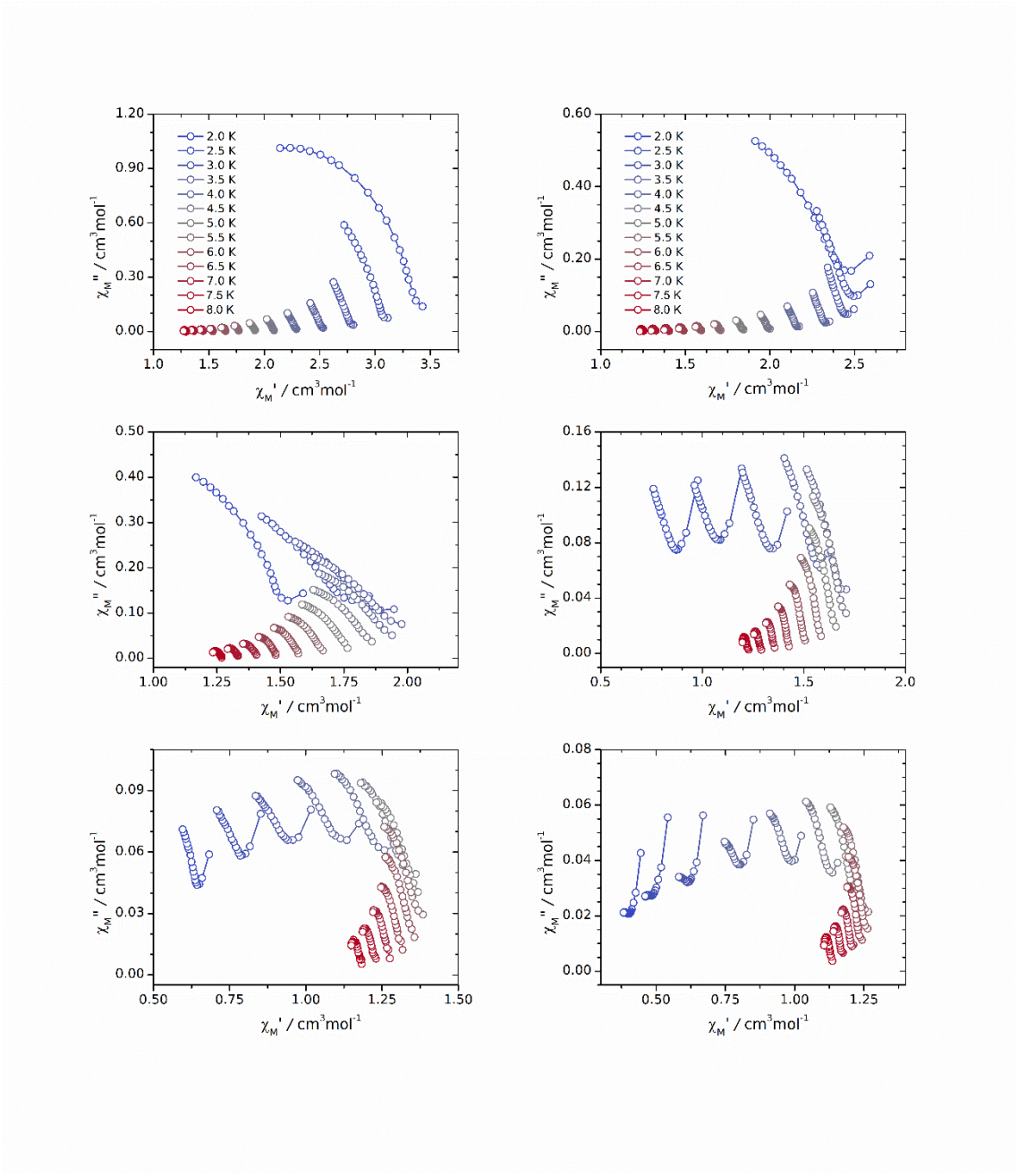

Figure S16. Argand diagrams of **2a** (left) and **2b** (right) under an external *dc* field of 1 (top), 2.5 (middle) and 5 kOe (bottom). Lines serve only as a visual guide.

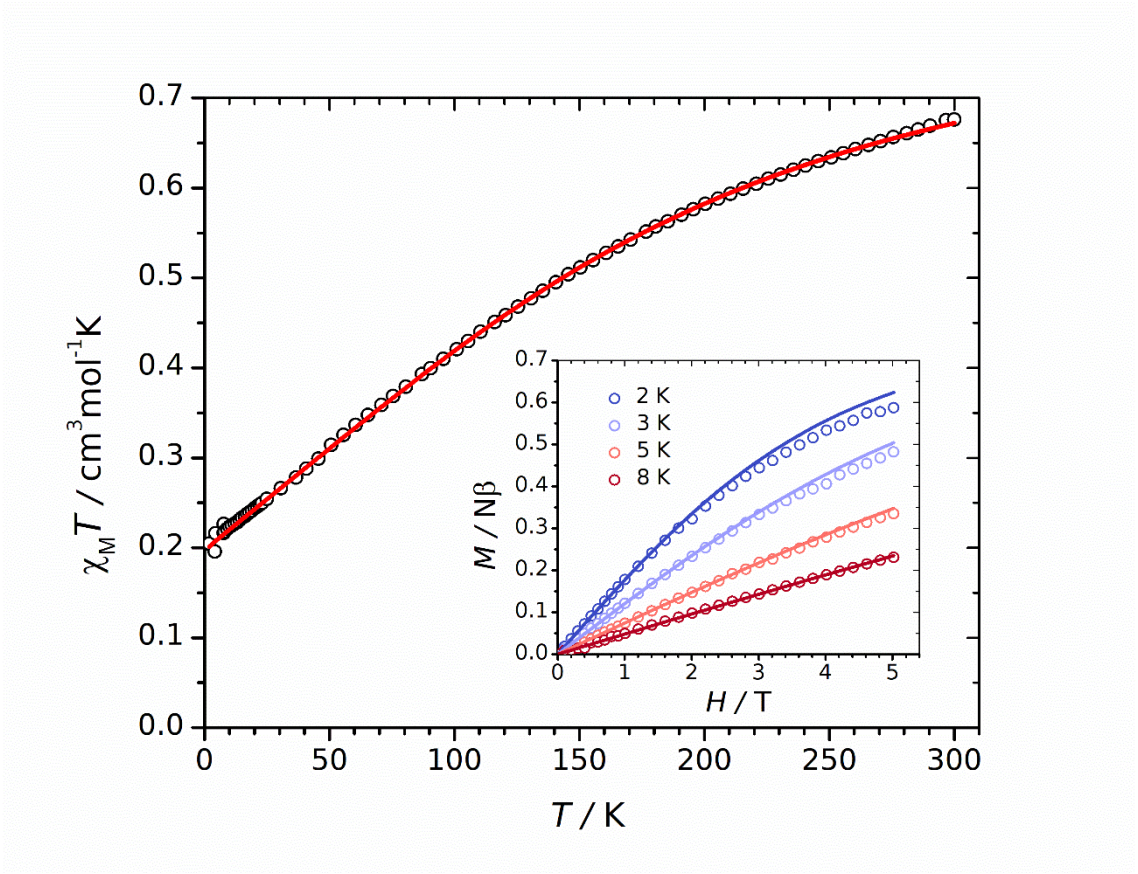

Figure S17. Temperature dependence of $\chi_M T$ measured at a 5 kOe *dc* field for **1**. Inset: Field dependence of magnetization at 2.0, 3.0, 5.0 and 8.0 K. The solid lines are the result of the best fit with Phi v3.1.6 (see main text for details).

Table S1. Parameters obtained from fitting *ac* susceptibility data of **1** to the generalized Debye model.

Field (Oe)	Temperature (K)	τ (s)	α
1000	2.00	$2.71(1) \times 10^{-4}$	$5.5(3) \times 10^{-2}$
1000	2.33	$1.86(1) \times 10^{-4}$	$5.6(3) \times 10^{-2}$
1000	2.67	$1.349(4) \times 10^{-4}$	$5.5(2) \times 10^{-2}$
1000	3.00	$1.001(5) \times 10^{-4}$	$4.8(3) \times 10^{-2}$
1000	3.33	$7.69(5) \times 10^{-5}$	$5.9(4) \times 10^{-2}$
1000	3.67	$6.03(10) \times 10^{-5}$	$5.1(10) \times 10^{-2}$
1000	4.00	$4.83(4) \times 10^{-5}$	$4.1(5) \times 10^{-2}$
1000	4.33	$3.96(6) \times 10^{-5}$	$4.8(8) \times 10^{-2}$
1000	4.67	$3.13(8) \times 10^{-5}$	$5.8(13) \times 10^{-2}$
1000	5.00	$2.60(6) \times 10^{-5}$	$3.9(12) \times 10^{-2}$
1000	5.33	$2.18(10) \times 10^{-5}$	$0.0(23) \times 10^{-2}$
1000	5.67	$1.60(15) \times 10^{-5}$	$9.3(30) \times 10^{-2}$
2000	2.00	$3.02(2) \times 10^{-4}$	$5.8(4) \times 10^{-2}$
2000	2.33	$2.02(3) \times 10^{-4}$	$4.7(10) \times 10^{-2}$
2000	2.67	$1.45(1) \times 10^{-4}$	$5.7(7) \times 10^{-2}$
2000	3.00	$1.08(1) \times 10^{-4}$	$5.8(7) \times 10^{-2}$
2000	3.33	$8.18(8) \times 10^{-5}$	$5.8(7) \times 10^{-2}$
2000	3.67	$6.44(6) \times 10^{-5}$	$4.8(6) \times 10^{-2}$
2000	4.00	$5.12(5) \times 10^{-5}$	$6.4(6) \times 10^{-2}$
2000	4.33	$4.11(5) \times 10^{-5}$	$6.0(7) \times 10^{-2}$
2000	4.67	$3.32(3) \times 10^{-5}$	$5.2(5) \times 10^{-2}$
2000	5.00	$2.74(7) \times 10^{-5}$	$5.0(13) \times 10^{-2}$
2000	5.33	$2.26(10) \times 10^{-5}$	$4.2(21) \times 10^{-2}$
2000	5.67	$1.83(4) \times 10^{-5}$	$4.8(9) \times 10^{-2}$

Table S2. QDPT/NEVPT2 calculated energies of Kramer doublets for **1** and main values of *g*-tensors in the three low-lying ones, calculated within the pseudo-spin $S = ½$ formalism. The angle θ is the deviation from the principal magnetization axes of the first KD.

KD	Energy (cm^{-1})	g_x	g_y	g_z	θ (°)
1	0.00	1.36865366	1.36789400	1.16249558	0
2	326.56	0.00572583	0.01677303	2.48956662	0.254
3	352.30	0.90157458	0.93482552	2.00724107	0.482
4	2287.92				
5	2635.55				
6	2701.48				
7	2903.34				

Table S3. Decomposition of the wave functions corresponding to the lowest atomic multiplet $J = 5/2$ in wave functions with a definite projection of the total moment on the quantization axis.

KD	ab initio state	$\|-5/2\rangle$	$\|-3/2\rangle$	$\|-1/2\rangle$	$\|+1/2\rangle$	$\|+3/2\rangle$	$\|+5/2\rangle$
1	1	0.6 %	0.0 %	57.7 %	0.9 %	0.0 %	40.9 %
	2	40.9 %	0.0 %	0.9 %	57.7 %	0.0 %	0.6 %
2	3	0.0 %	6.7 %	0.0 %	0.0 %	93.3 %	0.0 %
	4	0.0 %	93.3 %	0.0 %	0.0 %	6.7 %	0.0 %
3	5	20.1 %	0.0 %	27.3 %	14.2 %	0.0 %	38.5 %
	6	38.5 %	0.0 %	14.2 %	27.3 %	0.0 %	20.1 %

Table S4. SINGLE_ANISO computed crystal field parameters of the ground atomic multiplet J = 5/2 in **1**.

k	q	B_k^q
2	–2	–0.30417664197378E–01
2	–1	–0.26528268569014E–01
2	0	0.14359177891502E+01
2	1	0.26858208726643E–01
2	2	–0.14972726313285E–01
4	–4	–0.65467223074955E–02
4	–3	–0.12017178266198E+02
4	–2	0.22593186864573E–01
4	–1	0.13692029081035E–01
4	0	–0.57300658281820E+00
4	1	–0.28664792558835E–01
4	2	0.98881904610775E–02
4	3	–0.13793728367234E+02
4	4	–0.22885897020968E–01

Table S5. Matrix elements between states with opposite magnetization and between states arising from neighboring multiplets.

Matrix element	Average value
< 1.1+ | μ | 1.1- >	0.456091276514E+00
< 2.1+ | μ | 2.1- >	0.417215487510E-02
< 3.1+ | μ | 3.1- >	0.306119244444E+00
< 1.1+ | μ | 2.1+ >	0.347639702184E+00
< 1.1+ | μ | 2.1- >	0.613561757275E+00
< 2.1+ | μ | 3.1+ >	0.534891866073E+00
< 2.1+ | μ | 3.1- >	0.467820544305E+00
< 1.1+ | μ | 3.1+ >	0.409844855629E+00
< 1.1+ | μ | 3.1- >	0.446178822536E+00